LUNG DISEASE

Functional vascularized lung grafts for lung bioengineering

N. Valerio Dorrello,[1,2] Brandon A. Guenthart,[2,3]* John D. O'Neill,[2]* Jinho Kim,[2] Katherine Cunningham,[2] Ya-Wen Chen,[4,5] Mauer Biscotti,[3] Theresa Swayne,[6] Holly M. Wobma,[2] Sarah X. L. Huang,[4,5†] Hans-Willem Snoeck,[4,5,7,8] Matthew Bacchetta,[3] Gordana Vunjak-Novakovic[2,5‡]

End-stage lung disease is the third leading cause of death worldwide, accounting for 400,000 deaths per year in the United States alone. To reduce the morbidity and mortality associated with lung disease, new therapeutic strategies aimed at promoting lung repair and increasing the number of donor lungs available for transplantation are being explored. Because of the extreme complexity of this organ, previous attempts at bioengineering functional lungs from fully decellularized or synthetic scaffolds lacking functional vasculature have been largely unsuccessful. An intact vascular network is critical not only for maintaining the blood-gas barrier and allowing for proper graft function but also for supporting the regenerative cells. We therefore developed an airway-specific approach to removing the pulmonary epithelium, while maintaining the viability and function of the vascular endothelium, using a rat model. The resulting vascularized lung grafts supported the attachment and growth of human adult pulmonary cells and stem cell–derived lung-specified epithelial cells. We propose that de-epithelialization of the lung with preservation of intact vasculature could facilitate cell therapy of pulmonary epithelium and enable bioengineering of functional lungs for transplantation.

INTRODUCTION

Lung injury, whether acute or chronic, can lead to end-stage lung disease, a condition that affects millions of patients in the United States and accounts for approximately 400,000 deaths per year (*1*). Lung transplantation—the only definitive treatment for patients with end-stage lung disease—remains limited by a severe shortage of donor organs such that only 20% of patients waiting for a donor lung undergo transplantation (*2*). Strategies aimed at increasing the number of transplantable lungs would have an immediate and profound impact. In addition, early intervention with gene or cell therapy may offer even greater benefits by promoting lung repair and regeneration, thus slowing the progression of disease and ultimately avoiding the need for transplantation (*3*, *4*).

Gas exchange, the major function of the lung, requires close interaction between functional epithelium, intact alveolar-capillary membrane, and viable endothelium. Lung epithelium is highly susceptible to pathological insults and is specifically implicated in a number of congenital and acquired diseases. After injury, lung epithelium may either activate physiologic repair mechanisms or undergo aberrant remodeling. When repair mechanisms fail, epithelial-vascular-mesenchymal interplay can lead to dysfunctional wound healing dominated by fibrosis (*3*). The period following injury that determines the fate of lung epithelium may serve as an optimal window of time for therapeutic intervention to either promote healthy physiologic repair or allow for cell replacement. Tissue engineering strategies are currently under development to regenerate or replace injured lungs (*5*–*8*). Because of the extreme complexity of the lung, with its hierarchical three-dimensional architecture, diverse cellular composition, highly specialized extracellular matrix (ECM), and region-specific structure and function (*4*, *9*, *10*), bioengineering a functional lung is still an elusive goal (*11*, *12*). The lungs bioengineered by full decellularization and recellularization have shown a limited and temporary function, largely due to blood clotting and pulmonary edema, which have led to lung failure within a few hours following transplantation. To date, whole-organ engineering methods using lung grafts with denuded vascular networks have failed to produce functional grafts.

Given the essential need for intact and functional pulmonary vasculature (*13*), we developed an airway-specific approach to removing the pulmonary epithelium while preserving the lung vasculature, ECM, and other supporting cell types (for example, fibroblasts, myocytes, chondrocytes, and pericytes). We demonstrated the outcomes of our method by using a rodent lung model. Following lung cannulation, lungs were ventilated and perfused on an ex vivo lung perfusion (EVLP) circuit (Fig. 1A). A mild detergent solution was delivered intratracheally to an isolated single lung (Fig. 1B) to remove epithelial cells and obtain a functional vascularized lung scaffold (Fig. 1, C and D). We investigated the utility of this model in (i) removing pulmonary epithelial cells, (ii) maintaining and preserving pulmonary vascular integrity and function, and (iii) creating a vascularized lung scaffold supporting the delivery and engraftment of human airway epithelium and stem cell-derived lung-specified epithelial cells.

RESULTS

Lung de-epithelialization

Rat lung epithelium was removed by infusing a detergent solution only through the airway compartment. Following cannulation (fig. S1A), the

[1]Department of Pediatrics, Columbia University Medical Center, New York, NY 10032, USA. [2]Department of Biomedical Engineering, Columbia University Medical Center, New York, NY 10032, USA. [3]Department of Surgery, Columbia University Medical Center, New York, NY 10032, USA. [4]Columbia Center for Human Development, Columbia University Medical Center, New York, NY 10032, USA. [5]Department of Medicine, Columbia University Medical Center, New York, NY 10032, USA. [6]Herbert Irving Comprehensive Cancer Center, Columbia University Medical Center, New York, NY 10032, USA. [7]Columbia Center for Translational Immunology, Columbia University Medical Center, New York, NY 10032, USA. [8]Department of Microbiology and Immunology, Columbia University Medical Center, New York, NY 10032, USA.
*These authors contributed equally to this work.
†Present address: Center for Stem Cell and Regenerative Medicine, Brown Foundation Institute of Molecular Medicine, Houston, TX 77030, USA.
‡Corresponding author. Email: gv2131@columbia.edu

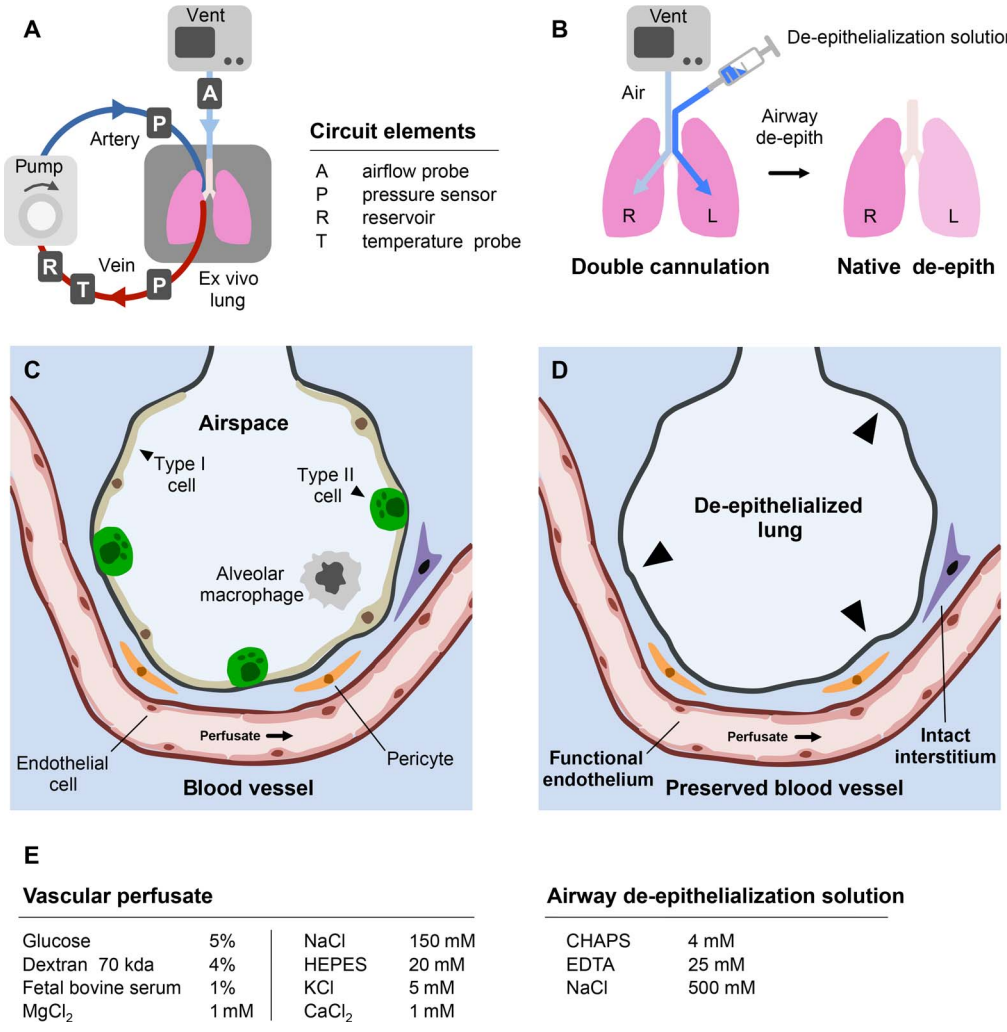

Fig. 1. Experimental setup of single lung airway de-epithelialization. (**A**) EVLP circuit and circuit elements. (**B**) Double lung cannulation method enabling ventilation of one lung (native) and airway de-epithelialization of contralateral lung (de-epith). R, right; L, left. (**C** and **D**) Schematic of experimental approach demonstrating (C) native airway, interstitium, and adjacent pulmonary vasculature and (D) denuded airway basement membrane following de-epithelialization with intact interstitium and preservation of vascular viability and function. (**E**) Components of vascular perfusate (see Materials and Methods for the complete list of components) and airway de-epithelialization solution.

animal was placed on an EVLP circuit (fig. S1B) and primed with venous blood. Ventilation on 21% oxygen resulted in normal gas exchange (ΔpO_2 = 121 ± 10 mmHg and ΔpCO_2 = −184 ± 6 mmHg), normal pH (pre-EVLP, 6.74 ± 0.3; EVLP, 7.4 ± 0.4), and a change to normal blood color (fig. S1C). The airway in one lung was isolated by cannulation of the main bronchus and ventilated to serve as control, whereas the other lung was subjected to de-epithelialization (Fig. 1B). Single lung ventilation maintained physiologic pH, pO_2, and pCO_2 (fig. S1C). Stable EVLP was achieved using a physiologic vascular perfusate composed of electrolytes, an energy substrate, and an oncotic regulator (Fig. 1E) that supported the lung during de-epithelialization (fig. S1D).

On the basis of previous studies in our laboratory (*14*), a 3-[(3-cholamidopropyl)dimethylammonio]-1-propane sulfonate (CHAPS) detergent–based solution was used for airway de-epithelialization. Concentrations of CHAPS and sodium chloride were optimized to enable efficient removal of the pulmonary epithelium while minimizing effects on the pulmonary interstitium and vasculature (Fig. 1E and fig. S2, A and C). To enhance distribution of the solution throughout the airway and to improve epithelial cell removal by physical agitation, we ventilated lungs at low tidal volumes (TV) [0.03 ml/100 g; normal value, 0.3 ml/100 g body weight (*15*)] and a high frequency [150 to 180 breaths per minute (bpm)], mimicking the high-frequency oscillatory ventilation (HFOV) used clinically in acute respiratory distress syndrome (ARDS) patients (movies S1 and S2).

Microscopic and Western blot analyses confirmed the removal of pulmonary epithelium (Fig. 2). In the conductive zone of the lung, histologic analysis indicated the removal of pseudostratified epithelium from the airway (Fig. 2, A to D). Immunostaining revealed the preservation of blood vessels retaining the endothelial cell marker Von Willebrand factor (vWF) and the interstitial fibroblast marker vimentin (fig. S3, A to D), adjacent to large airways stripped of the epithelial cell marker epithelial cell adhesion molecule (EpCAM) (Fig. 2, E and F). Similarly, in the respiratory zone, lung epithelium was removed from the bronchioles and alveoli (Fig. 2, G and H), with the preservation of small blood vessels retaining vWF and a significant reduction in the epithelial cell marker EpCAM (fig. S3, E and F), the alveolar type I cell marker aquaporin 5 (Aq5) (Fig. 2, I and J), and the type II cell marker

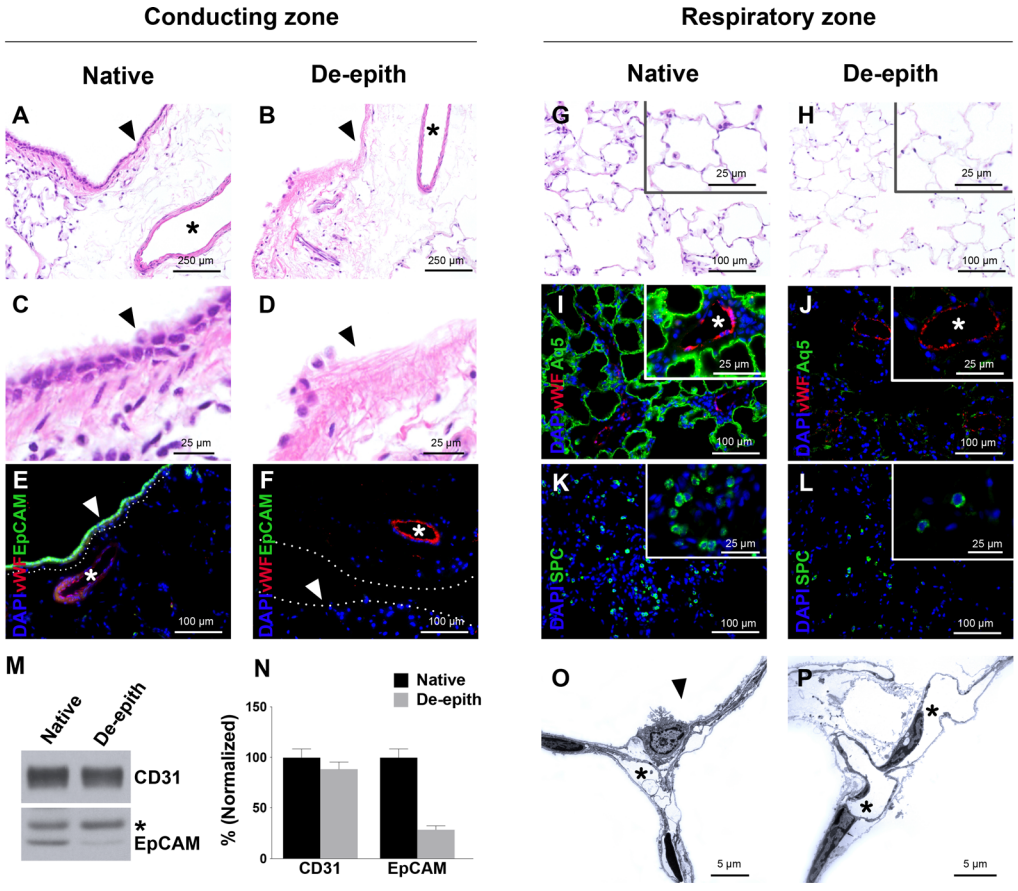

Fig. 2. Removal of pulmonary epithelium in conducting and respiratory zones. (**A** to **D**) Hematoxylin and eosin (H&E) staining of conducting zone in native and de-epithelialized lungs with intact pseudostratified epithelium (arrowheads) in the native lung (A and C) and denuded basement membrane (arrowheads) following the removal of respiratory epithelium in the de-epithelialized lung (B and D). Vessel is indicated by asterisk. (**E** and **F**) Immunofluorescence staining confirming the removal of bronchial epithelial cells by decreased EpCAM in de-epithelialized lung, with preservation of vessels indicated by vWF. (**G** and **H**) H&E staining of respiratory zone in native and de-epithelialized lungs. (**I** to **L**) Immunofluorescence staining confirmed the removal of alveolar type I cells by decreased Aq5, alveolar type II cells by decreased SPC, with preservation of vessels indicated by vWF in de-epithelialized lungs (J and L). (**M** and **N**) Western blot of CD31 and EpCAM from native and de-epithelialized lungs (asterisk indicates nonspecific band) (M). Quantification data indicate that de-epithelialized lungs contained five times less EpCAM than native ($n = 3$, values normalized to levels in native lung; error bars represent means ± SD of experimental values) (N). (**O** and **P**) TEM of native (O) and de-epithelialized (P) lungs showing intact microvessels and endothelial cell nuclei (asterisks) but absent alveolar cells (arrowheads) in de-epithelialized lungs.

surfactant protein C (SPC) (Fig. 2, K and L). Immunoblotting of epithelial (EpCAM) and endothelial (CD31) cell markers in de-epithelialized lungs verified preservation of intact endothelial cells, along with a significant loss (70%) of epithelial cells (Fig. 2, M and N, and fig. S3I). Furthermore, de-epithelialized lungs showed significant reductions in lung epithelial cell–specific markers, including Aq5 (bronchial epithelial and alveolar type I cell marker), SPC (alveolar type II cell marker), acetylated tubulin (ciliated cell marker) (*16*, *17*), and CC-10 (club cell marker) (fig. S3, G and H). Transmission electron microscopy (TEM) of de-epithelialized lungs showed denuded basement membrane due to the loss of alveolar epithelium and retention of both the alveolar-capillary basement membrane and microvascular endothelial cells in pulmonary capillaries (Fig. 2, O and P, and fig. S3, J to M).

Preservation of lung structure and ECM

Immunostaining, scanning electron microscopy, and quantitative analyses suggested that the de-epithelialized lung retains a native-like structure and ECM (Fig. 3). Distributions of ECM components retained in the de-epithelialized lung were similar to those in the native lung (Fig. 3A and fig. S4A), as well as the vessel structure (Fig. 3, B to E), histomorphology of airway submucosa and cartilage (Fig. 3, D to G), preservation of elastic fibers (Fig. 3, H and I), and architecture of the alveoli (fig. S4A). Further quantification of ECM components demonstrated no significant differences between native and de-epithelialized lungs with respect to hydroxyproline (HOP) ($P = 0.72$) and elastin ($P = 0.26$), indicating that de-epithelialization does not significantly reduce the concentrations of critical lung matrix components (Fig. 3J). Sulfated glycosaminoglycan (sGAG) content was decreased in de-epithelialized lungs compared to native lungs, although not significantly ($P = 0.15$). Quantification of DNA showed a 23.4% decrease in DNA content of de-epithelialized lungs compared to native lungs ($P = 0.04$) (Fig. 3J). In comparison, full decellularization resulted in the removal of >80% of DNA content compared to native lungs and 60% compared to de-epithelialized lungs ($P < 0.0001$, when compared to both native and de-epithelialized lungs). Scanning electronic microscopy confirmed the preservation of bronchial, alveolar, and vascular structures (Fig. 3K and

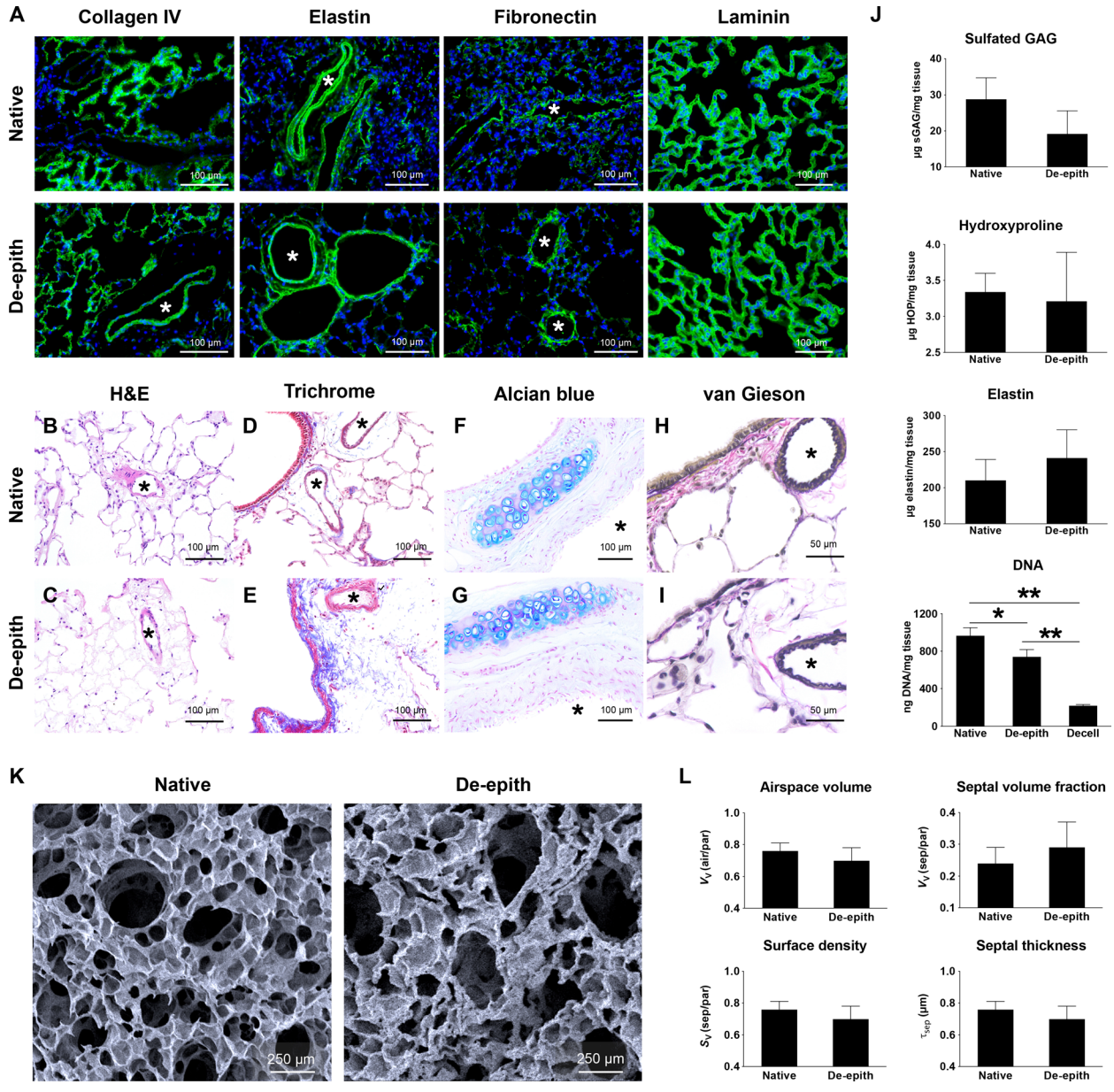

Fig. 3. Preservation of lung structure and ECM. (**A**) Immunofluorescence staining demonstrating preservation of collagen IV, elastin, fibronectin, and laminin in de-epithelialized lung. (**B** to **I**) H&E staining (B and C) and special staining of native and de-epithelialized lung: trichrome (D and E), Alcian blue (F and G), and van Gieson (H and I). (**J**) Quantification of sGAGs ($n = 3$; $P = 0.15$), HOP ($n = 3$; $P = 0.71$), elastin ($n = 3$; $P = 0.26$), and DNA (native, $n = 5$; de-epithelialized, $n = 5$; decellularized, $n = 4$; $^*P < 0.05$ and $^{**}P < 0.0001$). (**K**) Scanning electron microscopy of native and de-epithelialized lungs. (**L**) Morphometry and stereology of native and de-epithelialized lungs: airspace volume ($n = 3$; $P = 0.27$), septal volume fraction ($n = 3$; $P = 0.31$), surface density ($n = 3$; $P = 0.27$), and septal thickness ($n = 3$; $P = 0.98$). Data shown were analyzed by Student's t test. Error bars represent means ± SD of experimental values.

fig. S4, B to G). Morphometric and stereologic analyses did not show any significant differences between native and de-epithelialized lungs with respect to airspace volume fraction (native, 0.76 ± 0.05; de-epithelialized, 0.70 ± 0.08; $P = 0.27$; values are expressed as means ± SD throughout), septal volume fraction (native, 0.24 ± 0.05; de-epithelialized, 0.29 ± 0.08; $P = 0.31$), septal thickness (native, 7.1 ± 0.7 μm; de-epithelialized, 7.1 ± 0.5 μm; $P = 0.98$), and surface density (native, 0.067 ± 0.009; de-epithelialized, 0.081 ± 0.017; $P = 0.15$) (Fig. 3L). Because of the loss of alveolar surfactant and epithelial cells, dynamic lung compliance decreased after de-epithelialization (fig. S5, A to C).

Airway structure and smooth muscle function

Bronchial architecture, smooth muscle, and ECM components play pivotal roles in regulating gas exchange in the respiratory zone of the lung. Pentachrome staining of large bronchi showed de-epithelialized airways with histologic appearance otherwise similar to that of native airways. Collagen abundance in submucosal interstitium and airway cartilage is shown in yellow, with elastic fibers highlighted in black (Fig. 4, A and B). Smooth muscle actin (SMA) was observed in native and de-epithelialized lungs surrounding large airways and arteries (Fig. 4, C and D). Similarities in underlying airway smooth muscle

between native and de-epithelialized lungs were observed regardless of the presence or absence of airway epithelium (Fig. 4, C and D, arrowheads). Airway casts imaged by scanning electron microscopy showed no microscopic differences in airway structure between native and de-epithelialized lungs. Thin parallel striations visible along the length of bronchi within airway casts suggested that the natural wrinkles present in native lung airway lining (which render airways capable of accommodating increases in airway diameter up to 30% during inspiration) were also preserved following de-epithelialization (Fig. 4, E and F). Therefore, although the epithelial cells were effectively removed, it did not compromise the structure of the basement membrane lining of airways. Clusters of alveolar sacs were visible in airway casts of both native and de-epithelialized lungs (Fig. 4, E and F).

To assess the viability of airway smooth muscle cells and their responsiveness to physiological signals, we subjected de-epithelialized lungs to methacholine challenge similar to that used diagnostically for asthmatic patients (*18*, *19*). Following administration of methacholine, dynamic compliance significantly decreased in both native lungs [from 0.190 ± 0.046 ml/cmH_2O to 0.048 ± 0.007 ml/cmH_2O (reduction of 74.7 ± 8.7%)] and de-epithelialized lungs [from 0.065 ± 0.036 ml/cmH_2O to 0.031 ± 0.004 ml/cmH_2O (reduction of 45.3 ± 19%)]. These data demonstrated a clear bronchoconstrictive response to stimulation of muscarinic receptors in smooth muscle cells of the de-epithelialized lung airway (Fig. 4, G and H, and fig. S5, D to G). Following de-epithelialization, lungs showed reduced lung compliance before methacholine challenge (fig. S5, F and G).

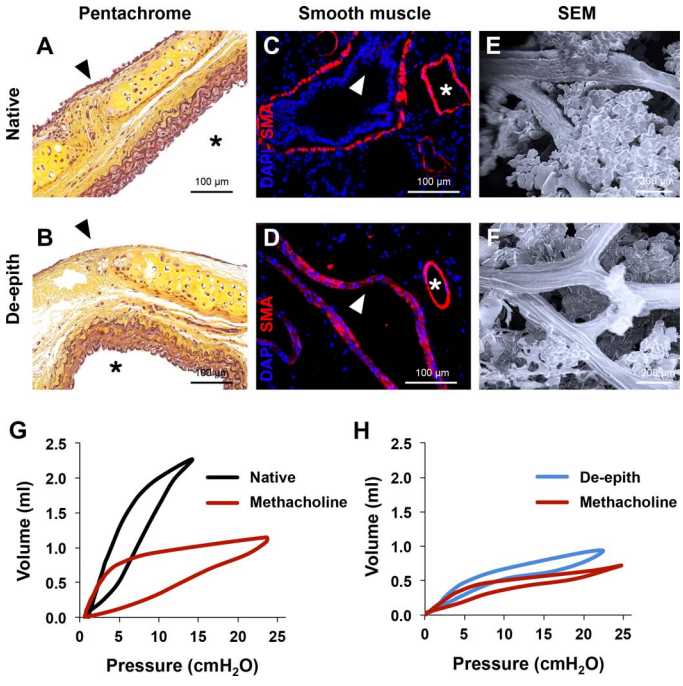

Fig. 4. Bronchial structure, viability, and function. Preservation of bronchial structure of native and de-epithelialized lungs (**A** to **F**). Pentachrome stain (A and B). SMA immunofluorescence staining (C and D). Airways are indicated by arrows, and vessels are indicated by stars. Scanning electron microscopy of airway casts (E and F). (**G** and **H**) Airway responsiveness during intravascular administration of methacholine measured by pressure-volume loops. Lung compliance in native (G) (0.190 ± 0.046 ml/cmH_2O; after methacholine, 0.048 ± 0.007 ml/cmH_2O; reduction of ~73.48 ± 8.704%) and de-epithelialized (H) (0.065 ± 0.036ml/cmH_2O; after methacholine, 0.031 ± 0.004 ml/cmH_2O; reduction of 45.28 ± 18.71%) lungs. Values are expressed as means ± SD.

Global preservation, viability, and function of pulmonary vasculature

Integrity of the pulmonary vascular bed and the alveolar-capillary membrane is critical for lung function (*13*, *20*). Immunostaining of de-epithelialized lung revealed preservation of markers for endothelial cells (vWF and CD31), smooth muscle cells (SMA), pericytes (NG2), tight junctions [zonula occludens–1 (ZO-1)], and gap junctions [connexin 43 (Cx43)] throughout the pulmonary vasculature (Fig. 5A and fig. S6A). The function of endothelial cells in the de-epithelialized lung was confirmed by the uptake of acetylated low-density lipoprotein (LDL) (Fig. 5B and fig. S6, B and C). The fractions of endothelial cells that were apoptotic in the TUNEL (terminal deoxynucleotidyl transferase–mediated deoxyuridine triphosphate nick end labeling) assay were comparable for the native and de-epithelialized lungs (n = 3, 82 of 521 and 33 of 385, respectively; P = 0.16) (Fig. 5C and fig. S6, D and E).

To assess the viability and function of vascular smooth muscle cells following de-epithelialization, a vasoconstrictor and a vasodilator were subsequently administered, while pressure was measured in the pulmonary artery (PA). De-epithelialized lungs demonstrated a marked vasoconstrictive response to endothelin-1, with an 89% pulmonary arterial pressure increase from baseline within 10 min. Response to the vasodilator treprostinil reversed most of the effects of endothelin-1 and demonstrated a notable decrease in arterial pressure after 20 min, resulting in an arterial pressure of 31.9% of baseline (Fig. 5D and fig. S6, F and G).

To assess alveolar-capillary barrier function in de-epithelialized lungs, 500-kDa FITC-dextran was administered via the PA and collected from the pulmonary veins (PVs) and airways (*21*). Native lungs and fully decellularized lungs retained 96 ± 6% and 21 ± 4%, respectively, of the total dextran administered to the vascular compartment. De-epithelialized lungs retained 62 ± 9.5% of the total dextran, indicating significant preservation of the alveolar-capillary barrier (Fig. 5E). Histologic assessment documented the differences between native, de-epithelialized, and fully decellularized lungs (Fig. 5F). To evaluate the integrity of the pulmonary microvasculature, 0.2-μm-diameter fluorescent microspheres were administered to de-epithelialized lungs through the PA and were seen in capillaries and larger vessels but not in either the alveoli or bronchoalveolar lavage (BAL) samples, indicating the integrity of the vascular tree (Fig. 5, G to I, and movies S3 and S4).

Recellularization of vascularized lung scaffolds

To assess whether de-epithelialized lungs could serve as a vascularized lung scaffold supporting therapeutic human cells, we developed a lung bioreactor system to investigate the engraftment and survival of human small airway epithelial cells (SAECs) and human-induced pluripotent stem cell (hiPSC)–derived lung-specified epithelial cells (*22*, *23*) within de-epithelialized lung scaffolds (Fig. 6A). SAECs were labeled with near-infrared (NIR) dye before intratracheal delivery to enable real-time transpleural imaging as a means of visualizing and monitoring cell distribution immediately after delivery (Fig. 6B). Twenty-four hours after delivery, carboxyfluorescein diacetate succinimidyl ester (CFSE)–labeled SAECs were detected throughout the tracheobronchial tree and in subpleural regions (Fig. 6C). Histological analysis of recellularized lungs confirmed the preservation of intact blood vessels (Fig. 6, D and E, fig. S7, A and B) and the presence of cells with squamous morphology attached to the basement membrane reconstituting the alveolar epithelium (Fig. 6, F and G, and fig. S7, C and D). Vascularized lung grafts were

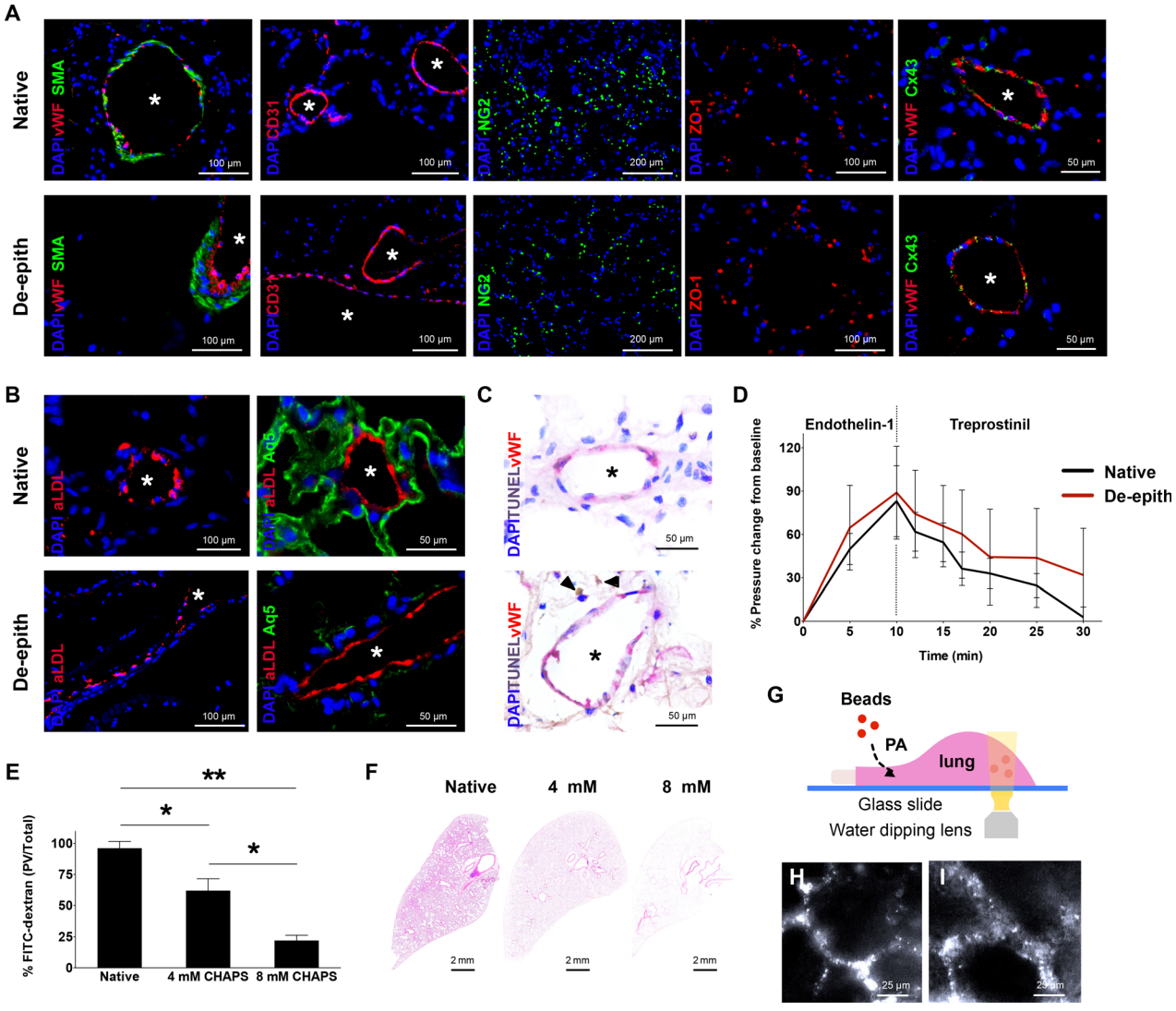

Fig. 5. Vascular preservation, viability, and function. (**A**) Immunofluorescence staining demonstrating the preservation of endothelial cells (vWF and CD31), vascular smooth muscle (SMA), pericytes (NG2), and tight and gap junction proteins (ZO-1 and Cx43) of the vascular bed following de-epithelialization. (**B**) Viability of endothelial cells by capture of acetylated LDL (aLDL) and loss of alveolar type I cells (Aq5) after de-epithelialization. (**C**) Nonapoptotic endothelial cells following de-epithelialization shown by TUNEL and vWF costaining; apoptotic cells (negative for vWF) in de-epithelialized lungs are indicated by arrowheads. (**D**) Intravascular administration of endothelin-1 and treprostinil demonstrating the preservation of vasoresponsiveness in native and de-epithelialized lungs (n = 3; Student's t test; error bars represent means ± SD of experimental values). (**E**) Integrity of the pulmonary vascular bed shown by quantification of fluorescein isothiocyanate (FITC)–conjugated dextran recovered from the pulmonary venous drainage in native lung, following 4 and 8 mM CHAPS treatment (n = 3 for each group; *P = 0.01 and **P < 0.01, Student's t test; error bars represent means ± SD of experimental values). (**F**) H&E histologic comparison of native lung and de-epithelialization by 4 and 8 mM CHAPS treatment. (**G** to **I**) Transpleural imaging to visualize pulmonary microvasculature. (G) Imaging setup with water-dipping lens. Images are captured during vascular perfusion of 0.2-μm fluorescent microspheres in (H) native and (I) de-epithelialized lungs (see movies S3 and S4). Blood vessels are indicated by asterisks.

effectively repopulated with CFSE-labeled SAECs. A total of 51.98 ± 2.78% epithelial cells in the lung graft were human (n = 3) (Fig. 6, H to J). Notably, vascularized lung scaffolds recellularized with SAECs displayed a level of metabolism similar to native lungs (P = 0.87) (Fig. 6K). DNA content of the recellularized lung was similar to that of the native lung (n = 3; native, 596.18 ± 386.12 ng per tissue biopsy; recellularized, 884.58 ± 596.37 ng per tissue biopsy; P = 0.40, Student's t test). Furthermore, 24 hours after recellularization, vascularized lung scaffolds demonstrated improved compliance (native, 0.066 ± 0.002 ml/cmH_2O; de-epithelialized, 0.017 ± 0.002 ml/cmH_2O; recellularized, 0.026 ± 0.0015 ml/cmH_2O). Compliance decreased by 74.2 ± 3.9% following de-epithelialization but increased by 53.4 ± 21% following recellularization by SAECs (Fig. 6L).

Survival and proliferation of delivered CFSE-labeled SAECs were assessed by immunostaining for Ki67 (proliferation marker) (Fig. 6M and fig. S7, E and F) and activated caspase-3 (apoptosis marker) (Fig. 6N). SAECs in recellularized lung maintain their proliferation state: 75 of 856 and 31 of 1030 Ki67-positive cells among CFSE-labeled SAECs and native cells, respectively (n = 3; P < 0.0001, Student's t test). The fractions of apoptotic cells in recellularized and intact lungs were comparable: 9 of 543 or 5 of 538 caspase-3–positive cells among CFSE-labeled SAECs, respectively (n = 3; P = 0.41, Student's t test).

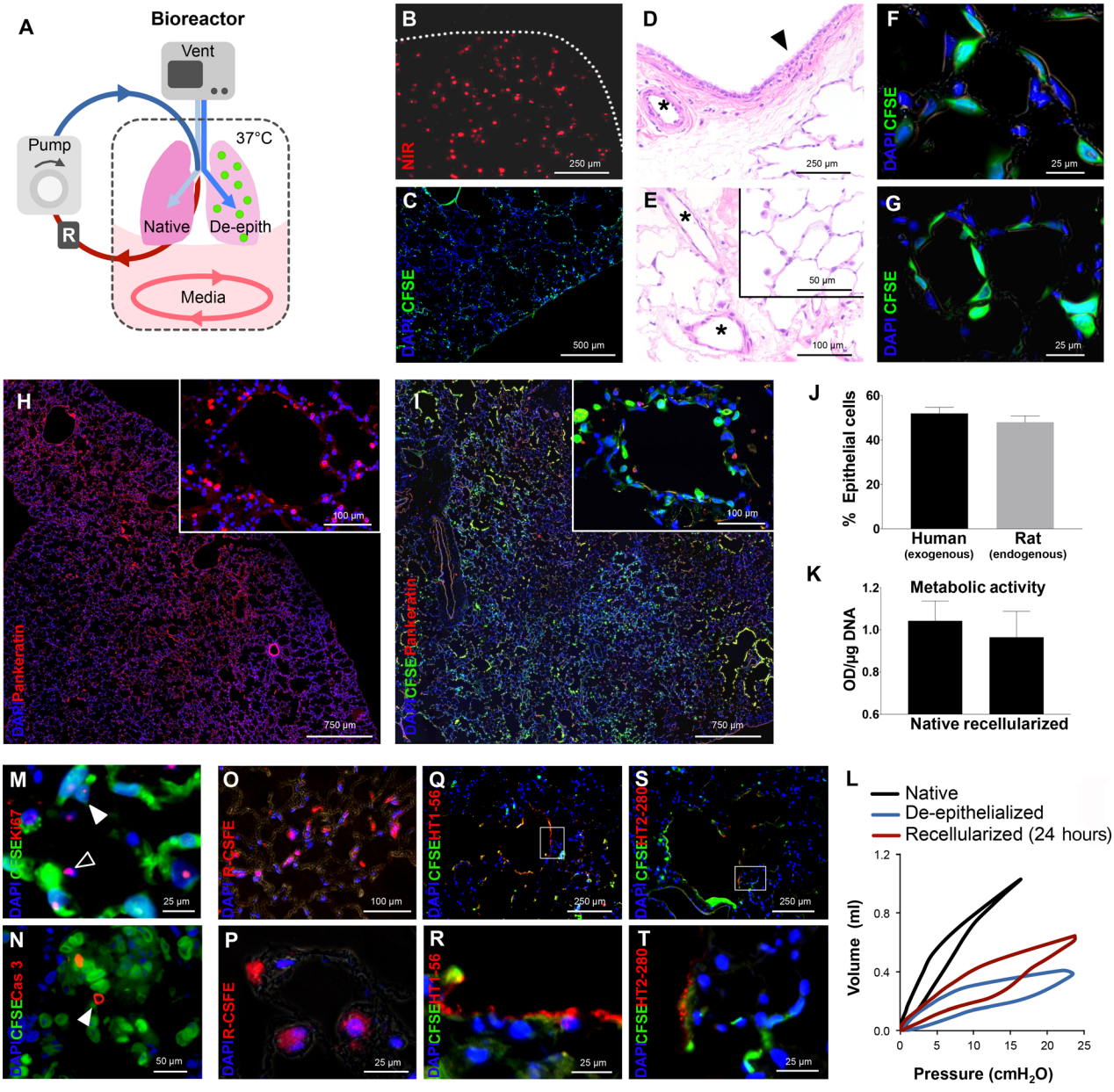

Fig. 6. Cell delivery, attachment, and viability in de-epithelialized lung. (**A**) Bioreactor schematic. R, reservoir of perfusate, cell culture medium; green circles, human SAECs or hiPSC-derived lung-specified epithelial cells delivered into de-epithelialized lung. (**B** and **C**) Delivery and attachment of SAECs in de-epithelialized lungs. Global distribution demonstrated with transpleural imaging of NIR-labeled cells (B) (dotted line indicates pleura). CFSE-labeled cells are distributed in the respiratory zone (C). (**D** to **G**) Lung section and histologic analysis of CFSE-labeled cells. H&E staining of native lung demonstrating intact pseudostratified respiratory epithelium (arrowhead) and vasculature (asterisk) (D) and of repopulated lung with intact native vasculature (asterisk) (E). CFSE-labeled SAECs attachment in the alveoli (F and G). (**H** to **J**) Immunostaining of native (H) and recellularized lungs with CFSE-labeled SAECs (I) with the epithelial marker Pankeratin. Inset: Higher-magnification images. Quantification of human and rat epithelial cells in recellularized lungs (n = 3; percentage of normalized to total Pankeratin-positive epithelial cells) (J). (**K**) Metabolic activity of native and recellularized lungs by resazurin assay (n = 3; P = 0.87, Student's t test; error bars represent means ± SD of experimental values). OD, optical density. (**L**) Dynamic lung compliance measured by pressure-volume loops of native, de-epithelialized, and recellularized lungs (n = 3; native, 0.066 ± 0.0022 ml/cmH_2O; de-epithelialized, 0.0169 ± 0.0021 ml/cmH_2O; recellularized, 0.0257 ± 0.0015 ml/cmH_2O; compliance decreased by ~74.20 ± 3.872% after de-epithelialization and increased by ~53.38 ± 20.83% after recellularization). Values are expressed as means ± SD. (**M** and **N**) Ki67 and caspase-3 (Cas 3) staining (indicated by filled arrowheads) demonstrating viable CFSE-labeled SAECs following 24 hours of culture in the bioreactor. Endogenous cells are indicated by the empty arrowhead. (**O** to **T**) Day 40 to 45 hiPSC-derived lung-specified epithelial cells, which were differentiated as described in Materials and Methods, were delivered into and attached in the de-epithelialized lung (O and P), expressing the human alveolar type I cell marker HT1-56 (Q and R) and the alveolar type II cell marker HT2-280 (S and T). (R) and (T) show higher magnification of boxed areas.

As a translational alternative to SAECs, vascularized lung scaffolds were recellularized with mRNA hiPSC–derived lung-specified epithelial cells fluorescently labeled at days 40 to 45. The cells contained 71.25 ± 3.34% $FOXA2^{+}NX2.1^{+}$ cells [over 4′,6-diamidino-2-phenylindole–positive ($DAPI^{+}$) population] of which approximately half expressed SPB (*22*, *23*). Twenty-four and forty-eight hours after intratracheal delivery, cells were uniformly distributed and attached to the alveolar basement membrane (Fig. 6, O to T). Notably, hiPSC-derived lung-specified epithelial cells attached to the native lung matrix (Fig. 6, O and P, and fig. S7, G and H) and expressed apical membrane markers specific to alveolar type I (HT1-56) (Fig. 6, Q and R) (*24*, *25*) and type II (HT2-280) cells (Fig. 6, S and T, and fig. S7, I to L) (*25*–*27*).

DISCUSSION

End-stage lung disease has a profound impact on the quality and duration of countless lives and represents a growing burden to health care systems worldwide (*28*). Despite meritorious efforts to better understand the pathogenesis of lung disease and identify targets and strategies to reverse disease trajectory, many patients suffer significant impairment and ultimately require lung transplantation (*2*). Although increasing the pool of donor lungs by implementing tissue engineering strategies has tremendous promise, several key obstacles have slowed the progress and even questioned the validity of this approach. The absence of functional vascular networks has been a major limitation in creating functional, nonthrombogenic lung constructs (*5*, *11*, *12*). Given the complexity of the lung, the needs for nutrient and oxygen delivery require vascular supply (*13*). Global lung function depends on the intricate and extensive capillary network, which could not be recapitulated or preserved using available bioengineering methods.

We demonstrate a transformative approach to obtaining functional vascularized lung grafts. By intratracheal targeting of the airway, we removed lung epithelium in a manner that preserves the surrounding cells, matrix, basement membrane, and vasculature. De-epithelialized lungs with intact, functional vasculature could serve as physiologic scaffold by (i) enabling the delivery of nutrients, oxygen, growth factors, and signaling molecules; (ii) providing key biophysical and mechanical signals via perfusion (flow and shear) and ventilation (strain); and (iii) maintaining the ECM (biochemical moieties, adhesion molecules, and matricryptic peptides) and the interstitial and support cells (fibroblasts, pericytes, endothelial, mesothelial, and lymphatic cells).

Previously established methods for decellularization of the entire organ were designed to remove both the epithelium and endothelium and could only be applied ex vivo (*5*, *11*, *12*, *14*). This study developed the first procedure for the removal of epithelium from the lung airway with the full preservation of vascular epithelium, which could be applied in vivo to treat diseases of lung epithelium (for example, ARDS and idiopathic pulmonary fibrosis). Whole lung scaffolds with an intact vascular network may also allow for recellularization using patient-specific cells and bioengineering of chimeric lungs for transplantation capable of gas exchange. In addition to the clinical potential, lung scaffolds lacking an intact epithelial layer but with functional vascular and interstitial compartments may also serve as a valuable physiological model for investigating (i) lung development, (ii) the etiology and pathogenesis of lung diseases involving pulmonary epithelium, (iii) acute lung injury and repair, and (iv) stem cell therapies.

We demonstrated the removal of airway epithelium by general histology (Fig. 2, A to D and G and H); immunostaining of EpCAM, Aq5, and SPC (Fig. 2, E and F and I to L); immunoblotting of EpCAM and other lung epithelial cell–specific markers (Fig. 2M and fig. S3G); and a 24% decrease in the DNA content (Fig. 3J). Given the cellular composition in the parenchyma of rat lung (43% endothelial cells, 32% interstitial cells, and 22% epithelial cells) (*29*), these results demonstrated that the treatment effects are well contained to the epithelium. Typically, full organ decellularization results in 75 to 98% DNA reduction, consistent with the depletion of all cell types (*14*, *30*–*32*).

Tissue ECM is known to provide the structural and mechanical support for resident cells, along with biochemical cues: growth factors, chemokines, and cytokines. The structure, composition, and mechanics of the ECM play major biological roles, making tissue-specific ECM an ideal scaffold for cell attachment, differentiation, and functional organization (*11*, *33*–*37*). In this respect, the proposed method results in retention of the lung architecture and matrix proteins, as evidenced by immunostaining (collagen IV, collagen I, elastin, fibronectin, and laminin), quantification of HOP and elastin (Fig. 3, A and J, and fig. S4A), scanning electron microscopy (Fig. 3K), and morphometric and stereologic analyses (Fig. 3L). Although not statistically significant, the measured decrease in sGAG content of de-epithelialized lungs (Fig. 3J) may be due to the loss of epithelial cell–associated sGAGs rather than matrix-bound sGAGs because our approach uses CHAPS at pH 8, known to be more protective of matrix-bound sGAGs compared to treatments with solutions at higher pH (*31*). The preserved matrix features in de-epithelialized lungs support diverse lung functions: elastic recoil during ventilation, cell adhesion, and barrier function.

The endothelial cells and functional vasculature were preserved in de-epithelialized lungs, as demonstrated by histology (Fig. 2, A and B), immunostaining for vWF (Fig. 2, E and F and I and J), and immunoblotting for CD31 (Fig. 2, M and N). The alveolar-capillary membrane remained intact, as shown by TEM and immunostaining for gap (Cx43) and tight (ZO-1) junctions (Figs. 2, O and P, and 5A and figs. S3, J to M, and S6A). Viability and function of endothelial cells in the macro- and microvasculature were shown by the capture of acetylated LDL (Fig. 5B and fig. S6, B and C). Blood vessels maintained responsiveness to vasoconstrictors/vasodilators, indicating that de-epithelialized lung scaffolds are capable of regulating blood flow (Fig. 5D). Integrity of the pulmonary vascular tree was well preserved, as demonstrated by the infusion of FITC-dextran (Fig. 5E) and microspheres (Fig. 5, H and I, and movies S3 and S4). The leakage of dextran in de-epithelialized lung scaffolds (~30%) was higher than that in an intact lung but much lower than that in a fully decellularized lung. This leakage, indicative of weakened endothelial tight junctions, may be transient and recoverable, given the presence of preserved endothelial cells and pericytes, an expectation that will need to be confirmed in long-term studies.

Ultimately, a challenge for using de-epithelialized lung as a scaffold for lung bioengineering is lung regeneration following infusion of fresh epithelial cells. Here, de-epithelialized lung scaffolds with preserved functional vasculature enabled the delivery and topographic distribution of several types of human cells, including human SAECs and hiPSC-derived lung-specified epithelial cells (Fig. 6). Cells attached throughout the distal lung, assuming a flattened morphology that normally precedes reconstitution of airway epithelium (Fig. 6, F and G). Fifty-two percent of all epithelial cells in our recellularized and vascularized lung scaffolds were human (Fig. 6, H to J). Following 24 hours of incubation in a bioreactor, cells were viable (Fig. 6, M and N) and metabolically active (Fig. 6K). Recellularized lungs with SAECs showed higher numbers of Ki67-positive cells compared to native lungs. This result is likely a reflection of the relatively low regeneration rate in native lungs (*4*) when compared to a cell line like SAECs.

Lung compliance showed a trend of improvement (Fig. 6L) that we attribute to recellularization and reconstitution of the alveolar membrane, rather than surfactant production, because we would not expect SAECs to produce surfactants over this time course. In previous studies of full decellularization and recellularization with rat lung fetal or neonatal epithelial cells (*11*, *12*), lung constructs showed production of SPC and SPA only at 4 to 5 days of bioreactor culture. Finally, hiPSC-derived lung-specified epithelial cells expressed markers specific to alveolar type I and type II cells (Fig. 6, Q to T), indicating that the vascularized lung scaffold supported their survival and phenotypic gene expression.

There are several limitations to the present study, which open new avenues for future research. To preserve the architecture and viability of the vascular compartment, we carefully titrated our de-epithelialization solution to only remove, as much as possible, epithelial cells. This titrated balance, which enabled vasculature preservation, also resulted in the retention of some endogenous epithelial cells. Nevertheless, we believe that these few remaining cells may also provide important instructive cues to cells newly introduced into the airway. Although our de-epithelialization approach targets airway epithelial removal, we cannot exclude some detergent leak in the vascular compartment. Although vascular viability and the attachment of exogenous cells confirmed a functional scaffold, long-term studies are needed to investigate the presence of residual detergent after de-epithelialization and its effects on scaffold functionality and cell viability. Immunological changes during de-epithelialization and recellularization were not investigated, given that human cells were studied in nude rats. It would be of interest to investigate the role of the innate immune system in chimeric lung constructs and define the host response to de-epithelialization in situ. In terms of recellularization, our hypothesis is that human pluripotent stem cell progenitor cells seeded into de-epithelialized regions of the lung, with the support of functional lung vasculature, will enable regeneration and remodeling of the donor lung. This could lead to a gradual increase in the fraction of the recipient's cells and contribute to global lung functionality. Unless patient-specific hiPSC cells can be used in the future, immunosuppression would be necessary during this transient period (extent and duration remain to be determined). Although this study used healthy lungs, the method is intended for application to injured lungs. We anticipate that diseased epithelium may have enhanced response to de-epithelialization and that the treatment may thus need to be shortened to achieve equivalent efficacy. Cell delivery and engraftment potential were demonstrated over a period of 24 to 48 hours. Vascularized lung scaffolds demonstrated a high level of recellularization, a parameter that can be experimentally manipulated by varying the number of human cells delivered. Additional studies are needed to determine optimal cell dosage and the degree to which exogenous cells expand and repopulate the recipient lung. Future studies are needed to evaluate the remodeling and function of recellularized lung scaffolds over prolonged periods and investigate their function in subsequent transplantation.

Lung decellularization has resulted in substantial advances in lung bioengineering and the ability to create acellular scaffolds for tissue engineering applications (*11*, *12*, *21*). We believe that our methodology can address some of the challenges that have slowed the progress in lung bioengineering by (i) preserving the vascular endothelium throughout the lung (from large vessels to capillaries) and (ii) targeting the removal of airway epithelium while maintaining structural and cellular components essential for lung repair. Further developments may involve the therapeutic use of de-epithelialization by targeting specific types of damaged/defective cells. Cell replacement therapy may have potential for repairing acutely injured epithelium (for example, following ARDS and acute injury), defective epithelium (for example, Hermansky-Pudlak syndrome and *SFTPC* disease), and conditions wherein the damaged epithelium activates aberrant remodeling (for example, chronic interstitial lung disease and Birt-Hogg-Dubé syndrome) (*3*). The use of patient-specific lung progenitor cells and the transplantation of chimeric organs may help mitigate rejection and offer a more personalized approach to lung transplantation (fig. S8) (*4*, *38*). Additionally, de-epithelialization could be applied to other organs with dual flow, such as the liver or kidney. In summary, the creation of de-epithelialized whole lungs with functional vasculature may open new frontiers in lung bioengineering and regenerative medicine.

MATERIALS AND METHODS

Animals

Lungs were harvested from 12-week-old Sprague-Dawley rats weighing 250 to 350 g (Charles River Laboratories). For recellularization experiments, 12-week-old Crl:NIH-*Foxn1*^{rnu} nude rats weighing 250 to 300 g (Charles River Laboratories) were used. All animal work was approved by the Columbia University Institutional Animal Care and Use Committee and complied with the National Research Council *Guide for the Care and Use of Laboratory Animals* (eighth edition). Animals were euthanized via intraperitoneal injection of sodium pentobarbital (140 mg/kg; Sigma-Aldrich) after heparin injection (1000 U/kg; Sagent Pharmaceuticals). Immediately after euthanasia, a median sternotomy was performed, and the trachea was exposed and cannulated using a 16- to 18-gauge catheter. Venous blood was collected from the inferior vena cava. The right ventricle was accessed, and the PA cannula (Harvard Apparatus) was placed directly in the PA and secured with a 4-0 Prolene tie. Next, an incision was made on the inferior aspect of the left ventricle, and mitral valve leaflets were dissected open. A PV cannula (Harvard Apparatus) was placed in the left ventricle and secured via a purse-string 4-0 Prolene suture to collect venous drainage. For dual lung cannulation, the right mainstem bronchus was isolated. A 5-0 Prolene tie was placed just inferior to the carina to ensure that the right lung remained isolated from the left. A small incision was made distal to the tie on the right mainstem bronchus, and a second cannula was placed and secured with 5-0 Prolene ties.

EVLP bioreactor

Bioreactor design and components

All tubing components were obtained from Pharmed (tube sizes L/S 14 and L/S 16). Pressure was monitored using a TruWave pressure transducer (Edwards Lifesciences) between the perfusion pump and the connection to the PA and PV cannulas. Perfusion was accomplished using a Masterflex L/S variable-speed roller pump (Masterflex). Initial flow rates were set to 2 to 5% of the estimated cardiac output, with a target PA pressure of <15 mmHg and a PV pressure of 3 to 5 mmHg. Ventilation was performed using a Small Animal Ventilator (Harvard Apparatus). Ventilation was initiated within the first 10 min of isolated EVLP, with the following initial settings: volume control mode; respiratory rate (RR), 25 bpm; TV, 0.6 ml/100 g; positive end-expiratory pressure, 5 cmH_2O; and FiO_2, 21%. During de-epithelialization, lungs were ventilated using HFOV (TV, 100 µl; RR, 150 to 180 bpm). Rat lungs were perfused with whole blood collected during animal harvest. Hemogas analysis was performed on blood before entry into the PA and on blood exiting

the PV cannula to assess gas exchange (fig. S1C). Blood gas analysis was performed using an epoc point-of-care blood analysis system (Epocal Inc.). Once gas exchange efficacy was confirmed, lungs were directly flushed with 20 ml of phosphate-buffered saline (PBS) containing heparin (50 U/ml) (Sigma-Aldrich) and 50 mg of methylprednisolone (APP Pharmaceuticals LLC), followed by perfusion with Hepes buffer [20 mM Hepes 150 mM NaCl, 1 mM $MgCl_2$, 5 mM KCl, 5% glucose, 1% fetal bovine serum, 1 mM $CaCl_2$, and 4% dextran (70 kDa)]. Inclusion of 4% dextran (70 kDa) maintains colloid osmotic pressure of 20 cmH_2O (*39*, *40*). Buffer pH was maintained between 7.35 and 7.45 and checked hourly.

EVLP monitoring

Pressure-volume loops of the lung were obtained during ventilation using a custom-configured measurement system. During the measurements, the trachea of the rat lung was attached to the measurement system connected to the ventilator that supported lung ventilation. The pressure-volume measurement system consisted of a pressure sensor (MPXV7002GC6U, Freescale Semiconductor), an airflow sensor (HAFBLF0200CAAX5, Honeywell), and a microcontroller (Arduino Uno). Pressure-volume data collected through the system were processed, and then pressure-volume loops were generated using MATLAB software (MathWorks). The quasi-static compliance (milliliters per centimeters of water) values of the lungs were determined from the inhalation curves of the pressure-volume loops (that is, quasi-static compliance = maximum volume/maximum pressure during inhalation).

Rat lung de-epithelialization

Freshly harvested lung tissues (n = 6 Sprague-Dawley rats and n = 6 nude rats) were mounted on EVLP, as described above. Both lungs were separately cannulated. The de-epithelialization solution was intratracheally injected into one lung, whereas the contralateral (control) lung was ventilated, as described above. The de-epithelialization solution contained 4 mM CHAPS (Sigma-Aldrich), 0.5 M NaCl (Sigma-Aldrich), and 25 mM EDTA (Sigma-Aldrich) in deionized water. During de-epithelialization, lungs were perfused with Hepes buffer, as described above. During de-epithelialization, both lungs were subjected to HFOV to allow more uniform oscillation of de-epithelialization solution within the treated lung. After 2 hours of treatment, airways were rinsed with washing solution {PBS and benzonase preconditioning buffer [50 mM tris-HCl (pH 8), bovine serum albumin (0.1 mg/ml), and 1 mM $MgCl_2$]}. The washing solution was infused through the airway cannula to the treated lung and let sit for the times indicated below. Next, the airway cannula was opened, and the washing solution was allowed to passively drain out. PBS washes were as follows: five fast washes (1 min) and two long washes (5 min). Subsequently, airways were rinsed twice for 10 min, each with benzonase precondition buffer, followed by treatment with benzonase (90 U/ml; Sigma-Aldrich) for 60 min to remove nucleic acids released from the cells, and then rinsed again with PBS (as above) before processing of the samples. Time for washing and benzonase treatment totaled 2 hours.

Rat lung complete decellularization

Freshly harvested lung tissues (n = 3 Sprague-Dawley rats) were mounted on EVLP, as described above. Both lungs were separately cannulated. The decellularization solution was intratracheally injected into one lung, whereas the contralateral (control) lung was ventilated, as described above. The decellularization solution contained 8 mM CHAPS (Sigma-Aldrich), 1 M NaCl (Sigma-Aldrich), and 25 mM EDTA (Sigma-Aldrich) in deionized water. During decellularization, lung perfusion and washing after treatment were performed as described in the de-epithelialization procedure.

Cell culture

Human SAECs (Lonza) were cultured and passaged by trypsinization and used before passage (P3). hiPSC-derived lung-specified epithelial cells were differentiated according to previously published methods (*22*, *23*). hiPSCs were generated from healthy human dermal fibroblasts using modified mRNA. mRNA hiPSCs were first prepared for definitive endoderm induction using activin A, followed by anterior foregut endoderm (AFE) induction with dual and sequential inhibition of bone morphogenetic protein (BMP) and transforming growth factor–β (TGF-β) and then by WNT and TGF-β signaling. AFE was further cultured with lung specification medium containing a WNT signaling agonist, fibroblast growth factor 10 (FGF10), FGF7, BMP4, and all-trans retinoic acid until day 15 of differentiation, followed by expanding with the WNT signaling agonist, FGF10, and FGF7 until day 25. From day 25, maturation components containing dexamethasone (Sigma-Aldrich), 8-bromo-cAMP (cyclic adenosine monophosphate) (R&D Systems), and 3,7-dihydro-1-methyl-3-(2-methylpropyl)-1*H*-purine-2,6-dione (Sigma-Aldrich) were added in addition to the WNT signaling agonist, FGF10, and FGF7. All cytokines were from R&D Systems, and all the small molecules were purchased from Tocris (R&D Systems).

Rat lung recellularization

Prepared de-epithelialized nude rat lungs (n = 5) were rinsed in culture medium with Antibiotic/Antimycotic (50×) (Life Technologies) and transferred to a tissue culture incubator for culture under standard sterile conditions at 37°C and 5% CO_2. Before recellularization, mRNA hiPSC–derived lung-specified epithelial cells at days 40 to 45 were dissociated with 0.05% trypsin gentle dissociation for 2 to 3 min, passed through a 40-μm cell strainer, and pelleted by centrifugation. Both SAECs and mRNA hiPSC–derived lung-specified epithelial cells were labeled with 5 to 10 μM CFSE (Abcam) or CellBrite NIR790 cytoplasmic membrane dye (Biotium) according to the manufacturer's instructions, and suspensions were prepared at a concentration of 5 to 10×10^6 cells/ml for SAECs and 2×10^6 cells/ml for hiPSC-derived lung-specified epithelial cells. Cells were intratracheally injected in five separate infusions of 1 ml, each with 1 min of liquid ventilation (RR, 5 bpm) between them. Immediately after cell injection, live transpleural imaging of NIR-labeled cells was performed using a custom imaging system developed in our laboratory that consists of a light-emitting diode (LED) excitation source (M780L3, Thorlabs), a camera (Zyla 4.2, Andor Technology Co.), and an objective (Plan N 10, Olympus). Three hours after injection, liquid ventilation was started (RR, 20 bpm). The medium in the airways was changed three times per day. Lungs were perfused with endothelial cell growth medium 2 with 20% fetal bovine serum (FBS), 500 nM hydrocortisone (Sigma-Aldrich), heparin (50 U/ml), and Antibiotic/Antimycotic (50×) at 1 cm^3/min. Culture periods generally varied from 24 to 48 hours.

Histopathologic analysis

The location of each lung section was standardized for every experiment by dividing the lung into six regions (upper right, middle right, lower right, upper left, middle left, and lower left regions) (fig. S2B). Specimens from control and de-epithelialized lungs were immediately fixed in cold phosphate–buffered 4% paraformaldehyde for 24 to 48 hours, embedded in paraffin, and sectioned at 3- or 5-μm thickness. All sections were stained for H&E and examined under light microscopy. Additional sections were stained for Alcian blue (pH 2.5), elastic van Gieson, trichrome, and pentachrome at the Department of Molecular Pathology at Columbia University.

Immunohistochemical staining

Lung sections were deparaffinized, subjected to boiling citrate buffer (pH 6.0) for antigen retrieval, and blocked with 10% normal goat serum in PBS for 2 hours at room temperature. Primary antibodies were added and incubated for 12 hours at 4°C or for 4 hours at room temperature. For all stains, the secondary antibody was diluted 1:200 and incubated for 1 hour at room temperature. Sections were mounted in a Vectashield Mounting Medium with DAPI (Vector Laboratories Inc.), coverslipped, and imaged using an Olympus FSX100 microscope (Olympus America Inc.). Late apoptosis was detected on tissue sections from rat lungs ($n = 3$) using TUNEL assay. Additional staining for vWF was conducted by the Herbert Irving Comprehensive Cancer Center (HICCC) molecular pathology services at Columbia University. A list of antibodies and dilutions used is provided in tables S1 and S2.

Immunofluorescence staining and analysis

Lung slices were deparaffinized, subjected to boiling citrate buffer (pH 6.0) for antigen retrieval, and permeabilized in PBS with 0.25% Triton X-100 and 5% fetal donkey or goat serum (Life Technologies) for 20 min. Samples were blocked in 10% fetal donkey or goat serum for 2 hours at room temperature. Sections were stained with one or a combination of two primary antibodies (table S1). After blocking, all stains were performed by incubating primary antibodies in staining/wash buffer (5% fetal goat serum in PBS) overnight at 4°C, followed by 3× 10-min wash. Sections were incubated with the corresponding secondary antibodies (table S2), diluted in staining/wash buffer for 2 hours at room temperature, washed twice for 10 min, incubated with DAPI for 5 min at room temperature, and mounted with Vectashield Mounting Medium (cat. #H-1000, Vector laboratories Inc.) for better preservation. Percentage of recellularization was quantified by analysis of immunofluorescence staining for Pankeratin (recognizes both human and rat epithelial cells) on nine sections of recellularized lungs from three independent experiments. The locations of each lung section were standardized and were randomly selected for analysis for every experiment (fig. S2B). The percentage of recellularization was calculated as the number of CFSE-labeled SAECs that stained positive for Pankeratin over the total number of Pankeratin-positive cells. Cell counts were quantified using the ImageJ particle analysis using previously described methods (*41*).

Immunoblotting analysis

Lung tissue samples were lyophilized and weighed. Consistent amounts of each sample (10 mg) were digested in a fixed volume of cold radioimmunoprecipitation assay (RIPA) buffer (Sigma-Aldrich) with protease/phosphatase inhibitors (Cell Signaling) for 1 hour at 4°C, followed by centrifugation at 14,000*g* for 30 min at 4°C to remove insoluble material. Cell pellets [SAECs and human umbilical cord endothelial cells (HUVECs)] were digested in RIPA buffer, and protein concentration was quantified via Bradford assay. Samples were reduced in Laemmli buffer (Novex, Life Technologies) for 10 min at 70°C. Samples were run on 4 to 12% polyacrylamide gels (Invitrogen); 30 μg of SAEC and HUVEC cell extracts were loaded as control. After electrophoresis, proteins were transferred to a nitrocellulose membrane or polyvinylidene difluoride membrane (Bio-Rad). Membranes were blocked for 1 hour in blocking/probing buffer (PBS with 5% nonfat dry milk, Bio-Rad; 0.1% Tween, Sigma-Aldrich). Primary antibodies were applied overnight in blocking/probing buffer, followed by 3× 10-min wash in PBS 0.1% Tween 20 (*42*). Secondary antibody was applied for 1 hour at room temperature at a dilution of 1:5000, followed by three washes, as described above. Protein signal was detected using an Odyssey 2.1 scanner. Antibody sources and dilutions are described in tables S1 and S2.

ECM proteins and DNA quantification

HOP quantification

HOP was quantified using the Hydroxyproline Assay Kit (Sigma-Aldrich). Briefly, lung parenchymal tissue samples were weighed, homogenized, and hydrolyzed in 12 M hydrochloric acid for 3 hours at 120°C. HOP was subsequently assayed according to the manufacturer's instructions.

sGAG quantification

sGAGs were quantified using the dimethylene blue (DMB) dye assay. Samples of lung parenchyma were weighed and digested in papain (125 μg/ml; Sigma-Aldrich) for 4 hours at 60°C. DMB dye (Sigma-Aldrich) was added to samples at a ratio of 8:1 (v/v). Absorbance was measured at 595 nm, with 540 nm as the reference wavelength, and normalized to sample dry weight.

Elastin quantification

Elastin was quantified using the Fastin Elastin Assay Kit (Biocolor). Briefly, lung parenchymal tissue samples were weighed, and water-soluble α-elastin was extracted via three hot 0.25 M oxalic acid extractions, which were combined for each sample. Elastin was assayed according to the manufacturer's instructions.

DNA quantification

DNA was quantified using the Quant-iT PicoGreen dsDNA (double-stranded DNA) Assay Kit (Invitrogen) according to the manufacturer's instructions. Briefly, lung parenchymal tissue samples were weighed and digested in papain (125 μg/ml; Sigma-Aldrich) for 4 hours at 60°C. Fluorescence was measured with excitation/emission at 480 nm/520 nm. DNA was quantified using a standard curve prepared with λ-phage DNA and normalized to sample dry weight.

Electron microscopy

Scanning electron microscopy

Samples obtained from the control and de-epithelialized lungs were fixed in formalin, rinsed in 70% EtOH, frozen, and lyophilized. Airway castings were obtained using a commercially available anatomical corrosion kit (Batson's #17, Polysciences Inc.) according to the manufacturer's instructions. Sections were imaged on a Hitachi S-4700 FE-SEM Zeiss GeminiSEM 300 with an accelerating voltage of 2.5 kV.

Transmission electron microscopy

Samples obtained from control and de-epithelialized lungs were fixed with a modified Karmovsky's fix (*43*) and a secondary fixation in reduced osmium tetroxide (*44*). Following dehydration, samples were embedded in an open analog resin. Ultrathin sections (65 nm) were contrasted with lead citrate stain (*45*) and viewed on a JEM 1400 electron microscope (JEOL USA Inc.) operated at 120 kV. Digital images were captured on a Veleta 2kx2k charge-coupled device (Olympus Soft Imaging Solutions) by electron microscopy at the Histology Core of Weill Cornell Medicine.

Morphometry and stereology

Three blocks (a few millimeters in thickness) were cut from native and de-epithelialized lungs of each animal ($n = 3$) at 4-mm intervals, so that the upper, middle, and lower regions of the left and right lungs were sampled (fig. S2B). Within each block, a 5-μm section was cut at a random start point. Sections were mounted and stained with H&E. Each entire lung section was imaged using a VS120 slide scanner (Olympus) at the objective lens magnification of ×20 and a pixel size of 0.347 μm.

Stereologic analysis was performed using the Fiji distribution (*46*) of ImageJ (*47*), the Multipurpose Grid macro version 1.0 (A. Mironov, University of Manchester; https://imagej.nih.gov/ij/macros/Multipurpose_grid.txt), and custom-written scripts, available at https://github.com/theresaswayne/stereology/releases/latest. Fields for stereologic analysis were selected randomly from each tissue section. To select fields, we overlaid a grid on an overview of the entire section using the VSI Reader plugin (O. Burri and R. Guiet, École Polytechnique Federale de Lausanne; http://biop.epfl.ch/TOOL_VSI_Reader.html). A Python script was written for ImageJ to select 40 random fields (1024 pixels × 1024 pixels in size) from the grid. Random numbers generated by the Python random module did not show artifactual patterns, as judged by visual inspection of random numbers rendered as pixel values in an image. The image data in each field were extracted using the VSI Reader. After removing empty fields, a subset of the selected fields was selected for further analysis, so that each part of the lung was represented equally in the data set. All measurements were carried out in a blinded fashion (fig. S9).

For volume fraction measurements, the Multipurpose Grid macro was used to overlay point grids on each image with random offsets (*48*). Intersections of points with alveolar airspace, alveolar duct airspace, septal tissue, and nonparenchyma were counted manually using the Multi-point tool in ImageJ. For large areas in which many points had to be counted, a region of interest was drawn around the area, and points were counted automatically using the particle analysis function in ImageJ. At least 119 images were analyzed for each group (native and de-epithelialized). The number of images analyzed and the grid point density were selected so that each structure was counted at least 200 times in each lung (*49*). Parenchymal volume was estimated by subtracting nonparenchymal points from the total number of points (*50*).

For surface density and septal thickness measurements, horizontal segmented lines were overlaid on each image with random offsets using the Multipurpose Grid macro (*48*). Intersections of septal surface with the lines and line end points lying on nonparenchyma were counted using the Multi-point tool. At least 119 images were analyzed for each group (native and de-epithelialized). The number of images analyzed, line density, and line length were set so that at least 200 intercepts were counted in each lung.

Parameters were calculated using the following formulas:For the volume ratio of alveolar septa to parenchyma (*11*, *51*)

$$V_V\left(\frac{\text{sep}}{\text{par}}\right) = \frac{P(\text{sep})}{P(\text{lung})} * \left(1 - \frac{P(\text{nonpar})}{P(\text{lung})}\right)$$

For the volume ratio of alveolar and ductal airspace to parenchyma (*11*, *51*)

$$Vv\left(\frac{\text{air}}{\text{par}}\right) = \frac{P(\text{alv}) + P(\text{alvduct})}{P(\text{lung})} * \left(1 - \frac{P(\text{nonpar})}{P(\text{lung})}\right)$$

For the surface density of alveolar septa with respect to parenchyma (*50*)

$$Sv\left(\frac{\text{sep}}{\text{par}}\right) = \frac{2*I(\text{sep})}{(P(\text{lung}) - P(\text{nonpar}))*L(p)}$$

For the mean septal thickness (*50*)

$$\tau(\text{sept}) = 2*\frac{Vv(\text{sep/paren})}{Sv(\text{sep/paren})}$$

where sep = alveolar septa, par = parenchyma, nonpar = nonparenchyma, alv = alveoli, alvduct = alveolar duct, $L(p)$ = line length per end point = 44.36 μm, P (structure) = number of points falling on the indicated structure, and I (structure) = number of intersections of test lines with the indicated structure. Scale factors were retrieved from the OlyVIA desktop VSI viewer (Olympus).

Each parameter was calculated using combined counts from all sections obtained from each lung. Groups were compared using Student's paired, two-tailed t test.

Functional assays

Acetylated LDL uptake

To assess the viability of vascular endothelium, rat lungs ($n = 3$) were perfused after de-epithelialization with acetylated LDL, Alexa Fluor 594 conjugate (L35353, Thermo Fisher Scientific) diluted 1:200 for 4 hours at the conclusion of each experiment. Following incubation, lungs were perfused with 1× PBS, fixed in cold phosphate–buffered 4% paraformaldehyde for 24 hours, embedded in paraffin, and sectioned at 5-μm thickness. Following deparaffinization and DAPI staining, slides were examined using a fluorescence microscope (Olympus FSX100).

Vascular responsiveness test

The effect of vasoconstrictor (endothelin-1) and vasodilator (treprostinil) on pulmonary vascular tone was tested in de-epithelialized ($n = 3$) and control ($n = 3$) rats. Heart-lung blocks were mounted on EVLP and mechanically ventilated, as described above. Lungs were perfused with a modified Krebs-Henseleit buffer (Sigma-Aldrich) with the addition of 1% fetal bovine serum, 4% dextran (70 kDa), and heparin (10 IU/ml). Buffer was continuously gassed with 95% CO_2/5% O_2 at 37°C to maintain pH 7.4. Endothelin-1 (20 nM; Sigma-Aldrich) was intravenously given into the PA cannula (*52*). PA pressure was continuously recorded, as previously described, to assess the changes in PA pressure. Infusion was stopped when 100% increase in PA pressure was achieved. Treprostinil (0.3 μM; United Therapeutics) was started, and infusion was stopped when 20% relaxation was recorded (*53*). Data were expressed as the percent change relative to the baseline pressure (mean ± SEM) during induced response to endothelin-1 and teprostinil infusions.

Bronchial responsiveness test

The effect of methacholine chloride (Methapharm) on bronchial muscular tone was tested in de-epithelialized ($n = 3$) and control ($n = 3$) rats. Heart-lung blocks were mounted on EVLP and mechanically ventilated, as described above. Lungs were perfused with modified Krebs-Henseleit buffer, as described above. Methacholine was added to the buffer at a concentration of 16 μg/kg per min for 15 min (*54*). Pressure-volume loops were recorded before infusion and at 5-, 10-, and 15-min time points from infusion. Plateau was reached at 10 min and maintained at 15 min.

FITC-dextran perfusion and BAL assay

FITC-dextran (500 kDa) (Sigma) perfusion assay was performed, as previously described (*21*). Dextran perfusion and BAL assay were performed on freshly isolated ($n = 3$), fully decellularized ($n = 3$), and de-epithelialized ($n = 3$) rat lungs.

Ex vivo lung vasculature perfusion with microspheres

Fluorescent microspheres (excitation/emission, 580 nm/605 nm; diameter, 0.2 μm; FluoSpheres F-8821, Thermo Fisher Scientific) were suspended in 1× PBS at a final concentration of 10^6 beads/ml. At the appropriate experimental time points, the microsphere solution was introduced into the vascular tree of lungs mounted on EVLP. Following the injection, rat lungs (n = 3) were placed on a petri dish, and the microspheres within the blood vessels were imaged using a custom-built microscope, which consisted of an excitation light source (M595L3, Thorlabs), an emission filter (FF02-641/75-25, Semrock), a 40× water immersion lens (CFI APO NIR 40×, 0.80 numerical aperture, 3.5-mm working distance; Nikon), and an sCMOS camera (Zyla 4.2, Andor).

Metabolic activity assay

Lung tissue from upper, middle, and lower regions were randomly selected from rat lungs cultured in the bioreactor for 24 to 48 hours (n = 3). Two-millimeter-diameter punch biopsies (n = 4) from each region were dissected in a sterile fashion, finely minced, and placed in a 96-well plate (BD Falcon). CellTiter-Blue Cell Viability Assay (Promega) reagent diluted 1:5 was added to each sample suspended in 100 μl of 1× Dulbecco's modified Eagle's cell culture medium with 10% FBS. Negative control contained only medium. The multiwell plate was covered with aluminum foil and incubated at 37°C with gentle shaking for 4 hours. Following incubation, well contents were transferred into new 96-well plates, and absorbance was measured at 570 nm and normalized to 600 nm. Following the metabolic activity assay, the DNA content of each sample was quantified using the Quant-iT PicoGreen dsDNA Assay Kit (Invitrogen) according to the manufacturer's instructions. Samples were digested in papain (250 μg/ml) for 4 hours at 60°C and mixed with PicoGreen reagent. Fluorescence emission was measured at 520 nm with excitation at 480 nm, and DNA was quantified using a standard curve.

Study design and statistical analysis

The study was conducted with the minimum number of animals to achieve reproducibility and statistical significance between time points (at least three animals per experiment).

Randomization of sampling

Samples of lung collected for histologic, microscopic, and pathologic analyses were collected at the end of each experiment according to a predetermined lung map (fig. S2B). A grid was overlaid over a section slide, and 20× magnified images were chosen for analysis after they had been numbered by a random number generator (www.random.org).

Blinded review

All analytical assessments were blinded to the maximum practical extent. Pathologic analysis was performed by a blinded independent expert to eliminate any bias.

Student's t tests were performed using Prism v6 (GraphPad). A value of $P < 0.05$ was considered statistically significant.

SUPPLEMENTARY MATERIALS

Supplementary material for this article is available at http://advances.sciencemag.org/cgi/content/full/3/8/e1700521/DC1

table S1. Primary antibodies.
table S2. Secondary antibodies.
fig. S1. Lung de-epithelialization.
fig. S2. Optimization of de-epithelialization solution in rodent lungs on EVLP.
fig. S3. Efficiency of de-epithelialization.
fig. S4. Preservation of lung structure and ECM.
fig. S5. Dynamic lung compliance.
fig. S6. Vascular viability and function after lung de-epithelialization.
fig. S7. Cell attachment and viability in de-epithelialized lung.
fig. S8. Schematic of ex vivo lung regeneration.
fig. S9. Outline of stereologic analysis.
movie S1. HFOV before de-epithelialization on EVLP.
movie S2. HFOV during de-epithelialization on EVLP.
movie S3. Native lung perfusion with microspheres.
movie S4. De-epithelialized lung perfusion with microspheres.

REFERENCES AND NOTES

1. J. Xu, S. L. Murphy, K. D. Kochanek, E. Arias, "Mortality in the United States, 2015" (National Center for Health Statistics Data Brief no. 267, 2016).
2. M. Valapour, M. A. Skeans, J. M. Smith, L. B. Edwards, W. S. Cherikh, K. Uccellini, A. K. Israni, J. J. Snyder, B. L. Kasiske, OPTN/SRTR 2015 annual data report: Lung. *Am. J. Transplant.* **17** (suppl. 1), 357–424 (2017).
3. M. F. Beers, E. E. Morrisey, The three R's of lung health and disease: Repair, remodeling, and regeneration. *J. Clin. Invest.* **121**, 2065–2073 (2011).
4. B. L. M. Hogan, C. E. Barkauskas, H. A. Chapman, J. A. Epstein, R. Jain, C. C. W. Hsia, L. Niklason, E. Calle, A. Le, S. H. Randell, J. Rock, M. Snitow, M. Krummel, B. R. Stripp, T. Vu, E. S. White, J. A. Whitsett, E. E. Morrisey, Repair and regeneration of the respiratory system: Complexity, plasticity, and mechanisms of lung stem cell function. *Cell Stem Cell* **15**, 123–138 (2014).
5. D. E. Wagner, N. R. Bonenfant, D. Sokocevic, M. J. DeSarno, Z. D. Borg, C. S. Parsons, E. M. Brooks, J. J. Platz, Z. I. Khalpey, D. M. Hoganson, B. Deng, Y. W. Lam, R. A. Oldinski, T. Ashikaga, D. J. Weiss, Three-dimensional scaffolds of acellular human and porcine lungs for high throughput studies of lung disease and regeneration. *Biomaterials* **35**, 2664–2679 (2014).
6. S. E. Gilpin, J. M. Charest, X. Ren, H. C. Ott, Bioengineering lungs for transplantation. *Thorac. Surg. Clin.* **26**, 163–171 (2016).
7. T. Tsuchiya, A. Sivarapatna, K. Rocco, A. Nanashima, T. Nagayasu, L. E. Niklason, Future prospects for tissue engineered lung transplantation: Decellularization and recellularization-based whole lung regeneration. *Organogenesis* **10**, 196–207 (2014).
8. H. Wobma, G. Vunjak-Novakovic, Tissue engineering and regenerative medicine 2015: A year in review. *Tissue Eng. Part B Rev.* **22**, 101–113 (2016).
9. D. E. Wagner, R. W. Bonvillain, T. Jensen, E. D. Girard, B. A. Bunnell, C. M. Finck, A. M. Hoffman, D. J. Weiss, Can stem cells be used to generate new lungs? Ex vivo lung bioengineering with decellularized whole lung scaffolds. *Respirology* **18**, 895–911 (2013).
10. T. H. Petersen, E. A. Calle, M. B. Colehour, L. E. Niklason, Matrix composition and mechanics of decellularized lung scaffolds. *Cells Tissues Organs* **195**, 222–231 (2012).
11. H. C. Ott, B. Clippinger, C. Conrad, C. Schuetz, I. Pomerantseva, L. Ikonomou, D. Kotton, J. P. Vacanti, Regeneration and orthotopic transplantation of a bioartificial lung. *Nat. Med.* **16**, 927–933 (2010).
12. T. H. Petersen, E. A. Calle, L. Zhao, E. J. Lee, L. Gui, M. B. Raredon, K. Gavrilov, T. Yi, Z. W. Zhuang, C. Breuer, E. Herzog, L. E. Niklason, Tissue-engineered lungs for in vivo implantation. *Science* **329**, 538–541 (2010).
13. C. T. Stabler, S. Lecht, M. J. Mondrinos, E. Goulart, P. Lazarovici, P. I. Lelkes, Revascularization of decellularized lung scaffolds: Principles and progress. *Am. J. Physiol. Lung Cell. Mol. Physiol.* **309**, L1273–L1285 (2015).
14. J. D. O'Neill, R. Anfang, A. Anandappa, J. Costa, J. Javidfar, H. M. Wobma, G. Singh, D. O. Freytes, M. D. Bacchetta, J. R. Sonett, G. Vunjak-Novakovic, Decellularization of human and porcine lung tissues for pulmonary tissue engineering. *Ann. Thorac. Surg.* **96**, 1046–1055 (2013).
15. K. P. Strohl, A. J. Thomas, P. St. Jean, E. H. Schlenker, R. J. Koletsky, N. J. Schork, Ventilation and metabolism among rat strains. *J. Appl. Physiol.* **82**, 317–323 (1997).
16. J. R. Rock, B. L. M. Hogan, Epithelial progenitor cells in lung development, maintenance, repair, and disease. *Annu. Rev. Cell Dev. Biol.* **27**, 493–512 (2011).
17. S. Westermann, K. Weber, Post-translational modifications regulate microtubule function. *Nat. Rev. Mol. Cell Biol.* **4**, 938–947 (2003).
18. P. J. Barnes, Pharmacology of airway smooth muscle. *Am. J. Respir. Crit. Care Med.* **158**, S123–S132 (1998).
19. R. O. Crapo, R. Casaburi, A. L. Coates, P. L. Enright, J. L. Hankinson, C. G. Irvin, N. R. MacIntyre, R. T. McKay, J. S. Wanger, S. D. Anderson, D. W. Cockcroft, J. E. Fish, P. J. Sterk, Guidelines for methacholine and exercise challenge testing-1999. This official statement of the American Thoracic Society was adopted by the ATS Board of Directors, July 1999. *Am. J. Respir. Crit. Care Med.* **161**, 309–329 (2000).
20. J. Bhattacharya, M. A. Matthay, Regulation and repair of the alveolar-capillary barrier in acute lung injury. *Annu. Rev. Physiol.* **75**, 593–615 (2013).
21. X. Ren, P. T. Moser, S. E. Gilpin, T. Okamoto, T. Wu, L. F. Tapias, F. E. Mercier, L. Xiong, R. Ghawi, D. T. Scadden, D. J. Mathisen, H. C. Ott, Engineering pulmonary vasculature in decellularized rat and human lungs. *Nat. Biotechnol.* **33**, 1097–1102 (2015).

22. S. X. L. Huang, M. N. Islam, J. O'Neill, Z. Hu, Y.-G. Yang, Y.-W. Chen, M. Mumau, M. D. Green, G. Vunjak-Novakovic, J. Bhattacharya, H.-W. Snoeck, Efficient generation of lung and airway epithelial cells from human pluripotent stem cells. *Nat. Biotechnol.* **32**, 84–91 (2014).
23. S. X. L. Huang, M. D. Green, A. T. de Carvalho, M. Mumau, Y.-W. Chen, S. L. D'Souza, H.-W. Snoeck, The in vitro generation of lung and airway progenitor cells from human pluripotent stem cells. *Nat. Protoc.* **10**, 413–425 (2015).
24. L. G. Dobbs, R. F. Gonzalez, L. Allen, D. K. Froh, HTI_{56}, an integral membrane protein specific to human alveolar type I cells. *J. Histochem. Cytochem.* **47**, 129–137 (1999).
25. Y.-W. Chen, S. X. Huang, A. L. de Carvalho, S.-H. Ho, M. N. Islam, S. Volpi, L. D. Notarangelo, M. Ciancanelli, J.-L. Casanova, J. Bhattacharya, A. F. Liang, L. M. Palermo, M. Porotto, A. Moscona, H.-W. Snoeck, A three-dimensional model of human lung development and disease from pluripotent stem cells. *Nat. Cell Biol.* **19**, 542–549 (2017).
26. C. E. Barkauskas, M. J. Cronce, C. R. Rackley, E. J. Bowie, D. R. Keene, B. R. Stripp, S. H. Randell, P. W. Noble, B. L. M. Hogan, Type 2 alveolar cells are stem cells in adult lung. *J. Clin. Invest.* **123**, 3025–3036 (2013).
27. L. G. Dobbs, R. Gonzalez, M. A. Matthay, E. P. Carter, L. Allen, A. S. Verkman, Highly water-permeable type I alveolar epithelial cells confer high water permeability between the airspace and vasculature in rat lung. *Proc. Natl. Acad. Sci. U.S.A.* **95**, 2991–2996 (1998).
28. *NHLBI Fact Book, Fiscal Year 2012* (2013).
29. D. M. Haies, J. Gil, E. R. Weibel, Morphometric study of rat lung cells. I. Numerical and dimensional characteristics of parenchymal cell population. *Am. Rev. Respir. Dis.* **123**, 533–541 (1981).
30. J. L. Balestrini, L. E. Niklason, Extracellular matrix as a driver for lung regeneration. *Ann. Biomed. Eng.* **43**, 568–576 (2015).
31. T. Tsuchiya, J. L. Balestrini, J. Mendez, E. A. Calle, L. Zhao, L. E. Niklason, Influence of pH on extracellular matrix preservation during lung decellularization. *Tissue Eng. Part C Methods* **20**, 1028–1036 (2014).
32. S. E. Gilpin, J. P. Guyette, G. Gonzalez, X. Ren, J. M. Asara, D. J. Mathisen, J. P. Vacanti, H. C. Ott, Perfusion decellularization of human and porcine lungs: Bringing the matrix to clinical scale. *J. Heart Lung Transplant.* **33**, 298–308 (2014).
33. S. E. Dunsmore, D. E. Rannels, Extracellular matrix biology in the lung. *Am. J. Physiol.* **270**, L3–L27 (1996).
34. A. F. G. Godier-Furnémont, T. P. Martens, M. S. Koeckert, L. Wan, J. Parks, K. Arai, G. Zhang, B. Hudson, S. Homma, G. Vunjak-Novakovic, Composite scaffold provides a cell delivery platform for cardiovascular repair. *Proc. Natl. Acad. Sci. U.S.A.* **108**, 7974–7979 (2011).
35. S. F. Badylak, D. Taylor, K. Uygun, Whole-organ tissue engineering: Decellularization and recellularization of three-dimensional matrix scaffolds. *Annu. Rev. Biomed. Eng.* **13**, 27–53 (2011).
36. H. C. Ott, T. S. Matthiesen, S.-K. Goh, L. D. Black, S. M. Kren, T. I. Netoff, D. A. Taylor, Perfusion-decellularized matrix: Using nature's platform to engineer a bioartificial heart. *Nat. Med.* **14**, 213–221 (2008).
37. C. C. W. Hsia, Comparative analysis of the mechanical signals in lung development and compensatory growth. *Cell Tissue Res.* **367**, 687–705 (2017).
38. C. Yang, J. Jiang, X. Yang, H. Wang, J. Du, Stem/progenitor cells in endogenous repairing responses: New toolbox for the treatment of acute lung injury. *J. Transl. Med.* **14**, 47 (2016).
39. R. Ragette, C. Fu, J. Bhattacharya, Barrier effects of hyperosmolar signaling in microvascular endothelium of rat lung. *J. Clin. Invest.* **100**, 685–692 (1997).
40. J. Lindert, C. E. Perlman, K. Parthasarathi, J. Bhattacharya, Chloride-dependent secretion of alveolar wall liquid determined by optical-sectioning microscopy. *Am. J. Respir. Cell Mol. Biol.* **36**, 688–696 (2007).
41. F. Papadopulos, M. Spinelli, S. Valente, L. Foroni, C. Orrico, F. Alviano, G. Pasquinelli, Common tasks in microscopic and ultrastructural image analysis using ImageJ. *Ultrastruct. Pathol.* **31**, 401–407 (2007).
42. N. V. Dorrello, A. Peschiaroli, D. Guardavaccaro, N. H. Colburn, N. E. Sherman, M. Pagano, S6K1- and βTRCP-mediated degradation of PDCD4 promotes protein translation and cell growth. *Science* **314**, 467–471 (2006).
43. S. K. Ainsworth, S. Ito, M. J. Karnovsky, Alkaline bismuth reagent for high resolution ultrastructural demonstration of periodate-reactive sites. *J. Histochem. Cytochem.* **20**, 995–1005 (1972).
44. W. de Bruijn, Glycogen, its chemistry and morphologic appearance in the electron microscope. I. A modified OsO_4 fixative which selectively contrasts glycogen. *J. Ultrastruct. Res.* **42**, 29–50 (1973).
45. J. H. Venable, R. Coggeshall, A simplified lead citrate stain for use in electron microscopy. *J. Cell Biol.* **25**, 407–408 (1965).
46. J. Schindelin, C. T. Rueden, M. C. Hiner, K. W. Eliceiri, The ImageJ ecosystem: An open platform for biomedical image analysis. *Mol. Reprod. Dev.* **82**, 518–529 (2015).
47. C. A. Schneider, W. S. Rasband, K. W. Eliceiri, NIH Image to ImageJ: 25 years of image analysis. *Nat. Methods* **9**, 671–675 (2012).
48. H. J. G. Gundersen, E. B. Jensen, The efficiency of systematic sampling in stereology and its prediction. *J. Microsc.* **147**, 229–263 (1987).
49. C. C. W. Hsia, D. M. Hyde, M. Ochs, E. R. Weibel, An official research policy statement of the American Thoracic Society/European Respiratory Society: Standards for quantitative assessment of lung structure. *Am. J. Respir. Crit. Care Med.* **181**, 394–418 (2010).
50. C. Brandenberger, M. Ochs, C. Muhlfeld, Assessing particle and fiber toxicology in the respiratory system: The stereology toolbox. *Part. Fibre Toxicol.* **12**, 35 (2015).
51. C. Mühlfeld, L. Knudsen, M. Ochs, Stereology and morphometry of lung tissue. *Methods Mol. Biol.* **931**, 367–390 (2013).
52. M. J. Horgan, J. M. Pinheiro, A. B. Malik, Mechanism of endothelin-1-induced pulmonary vasoconstriction. *Circ. Res.* **69**, 157–164 (1991).
53. C. Benyahia, K. Boukais, I. Gomez, A. Silverstein, L. Clapp, A. Fabre, C. Danel, G. Leséche, D. Longrois, X. Norel, A comparative study of PGI2 mimetics used clinically on the vasorelaxation of human pulmonary arteries and veins, role of the DP-receptor. *Prostaglandins Other Lipid Mediat.* **107**, 48–55 (2013).
54. F. Petak, Z. Hantos, A. Adamicza, T. Asztalos, P. D. Sly, Methacholine-induced bronchoconstriction in rats: Effects of intravenous vs. aerosol delivery. *J. Appl. Physiol.* **82**, 1479–1487 (1997).

Acknowledgments: We thank M. C. Nostro (University Health Network, Toronto) and S. Kernie (Columbia University) for critically reading the manuscript, M. Pagano's laboratory at New York University for Western blot reagents and technical support, S. Halligan for administrative and logistical support, H. K. Lim of Rockefeller University for stem cell marker quantification, L. Cohen-Gould of Electron Microscopy and Histology Core of Weill Cornell Medicine for TEM imaging (NIH grant S10RR027699), and D. Queen and A. Taubman for experimental assistance. Stereologic analysis was performed in the Confocal and Specialized Microscopy Shared Resource of the HICCC, Columbia University (NIH grant P30 CA013696). **Funding:** This work was supported by NIH (P41 EB002520 and U01HL134760 to G.V.-N.), Driscoll Children's Fund and Hearts of ECMO (Extracorporeal Membrane Oxygenation) (to N.V.D.), the Mikati Foundation (to G.V.-N.), and the Richard Bartlett Foundation (to M.B.). **Author contributions:** N.V.D., M. Bacchetta, and G.V.-N. designed the study. N.V.D., B.A.G., M. Biscotti, J.D.O., J.K., T.S., K.C., Y.-W.C., and H.M.W. performed the experiments. S.X.L.H. provided the hiPSC-derived lung-specified epithelial cells. N.V.D., B.A.G., J.D.O., M. Bacchetta, K.C., Y.-W.C., and G.V.-N. coanalyzed the data. N.V.D., J.D.O., B.A.G., K.C., H.-W.S., M. Bacchetta, and G.V.-N. wrote the manuscript. **Competing interests:** H.-W.S., S.X.L.H., and Y.-W.C. are authors on a patent application related to this work filed by Columbia University (application no. PCT/US2013/051913, filed 24 July 2013). The other authors declare that they have no other competing interests. **Data and materials availability:** All data needed to evaluate the conclusions in the paper are present in the paper and/or the Supplementary Materials. Additional data related to this paper may be requested from the authors.

Submitted 16 February 2017
Accepted 28 July 2017
Published 30 August 2017
10.1126/sciadv.1700521

Citation: N. V. Dorrello, B. A. Guenthart, J. D. O'Neill, J. Kim, K. Cunningham, Y.-W. Chen, M. Biscotti, T. Swayne, H. M. Wobma, S. X. L. Huang, H.-W. Snoeck, M. Bacchetta, G. Vunjak-Novakovic, Functional vascularized lung grafts for lung bioengineering. *Sci. Adv.* **3**, e1700521 (2017).